

Gravity balls in induced gravity model— ‘gravitational lens’ effects

M. V. Safonova¹ and D. Lohiya²

Dept. Physics & Astrophysics,
 University of Delhi, Delhi-7, India

In non-minimally coupled effective gravity theories one can have non-topological solitonic solutions. A typical solution is a spherical region with $G_{eff} = 0$ outside and having the canonical Newtonian value inside. Such a spherical domain (gravity-ball) is characterized by an effective index of refraction which causes bending of light incident on it. The gravity ball thus acts as a spherical lens. We consider the gravity ball to be of a size of a typical cluster of galaxies and show that even empty (without matter) gravity ball can produce arc-like images of the background source galaxy. In the case of background random galaxy field the ball produces distortions (‘shear’) of that field. We also obtained constraints on the size of the large gravity ball, which can be inferred from the existing observations of clusters with arcs.

1. Introduction

One of the remarkable results of field theory is the existence of stable classical states of a field with non-vanishing energy. Such fields include topological solitons, domain walls, strings and monopoles. In addition to these field configurations, which are stabilized by their topological properties, non-topological solitons (NTS) produced by scalar fields have appeared in the literature and their relevance to cosmology has been assessed (for example, [1]). Variations on this theme include cosmic neutrino balls [2], [3], Q-balls [4] and soliton stars [5]. NTS are rendered stable by the existence of a conserved Noether charge carried by the fields confined to a finite region of space. The theory essentially contains an additive quantum number N carried either by a spin-1/2 field ψ (for example, fermion number), or a spin-0 complex field φ . In addition there is a scalar field σ residing at $\sigma = 0$ in the normal (true) vacuum state and at $\sigma = \sigma_0$ in the local (false) vacuum state. The soliton contains the interior in which $\sigma \approx \sigma_0$, a shell of width $\approx \mu^{-1}$ over which σ changes from σ_0 to 0 (μ being the mass associated with the scalar field), and finally the exterior that is the true vacuum. The N -carrying field ψ , or φ , is confined to the interior where it is effectively massless at the local minimum of the potential, $\sigma = \sigma_0$ (at the global minimum, $\sigma = 0$ the field (ψ or φ) has a non-vanishing mass, m). This leads to a stable configuration of massless particles trapped inside a region with $\sigma = \sigma_0$ separated from the true vacuum $\sigma = 0$ by a wall of thickness $\approx \mu^{-1}$. Confinement occurs for all particle states that are not on-shell in the exterior region. The NTS will be stable as long as the kinetic energy E_k of the particles inside the bag is less than

E_{free} —the minimum on-shell energy in the exterior region. In the scenario of formation of the NTSs upon the spontaneous breaking of discrete symmetry, two regions of different vacua (true and false) are separated by a domain wall. A bubble of true vacuum forms in a domain trapped in a false ground state. The false state collapses due to the surface tension of the boundary. The collapse is inhibited, however, by the pressure exerted by (for example) massless fermions, which cannot leave the interior of the bubble since their energy is less than their mass outside the bubble. This was explicitly demonstrated by Lee and Wick [6],[7].

The role of scalar fields in effective gravity models stems from the classical work of Brans and Dicke. In these approaches the gravitational action is induced by a coupling of the scalar curvature with a function of a scalar field. Lee and Wick’s results can be carried over to a curved spacetime with a scalar curvature non-minimally coupled to σ in the class of theories described by the effective action

$$S = \int \sqrt{-g} d^4x \left[U(\sigma)R + \frac{1}{2}(\partial_\mu\sigma)^2 - V(\sigma) + \tilde{U}(\sigma) (m\bar{\psi}\psi + \bar{\psi}\gamma^\mu\partial_\mu\psi) \right] \quad (1)$$

Establishing σ_{in} and σ_{out} as the interior and exterior values of σ , the effective gravitational constant would be given by

$$G_{eff}^{in} = [U(\sigma_{in})]^{-1}$$

and

$$G_{eff}^{out} = [U(\sigma_{out})]^{-1}$$

If U goes to infinity at some point, defined as $\sigma = 0$ without loss of generality, the theory gives rise to a solution with a spatial variation of the effective gravitational constant, $G_{eff}^{out} = 0$ and $G_{eff}^{in} = const$. This

¹e-mail: rita@iucaa.ernet.in

²e-mail: dlohiya@ducos.ernet.in

would be a generic feature of a Lee-Wick solution in which the scalar field is non-minimally coupled to the scalar curvature. It would give rise to a stable “ball of gravity”. In the present paper, we examine this special kind of NTS solutions referred to as G-balls [8].

A gravity ball is characterised by an effective refractive index in its interior. This would cause bending of light incident on it. The G-ball thus acts as a spherical lens. Gravitational lensing (GL) is a powerful tool in exploring the Universe. The topic has presently matured to the stage where GL is applied by astronomers for a variety of purposes and, in particular, it is providing an exciting new probe of detecting exotic objects in the Universe (may be described by the matter fields which are not detected yet) as well as of testing alternative theories of gravity. Proposals have been made to discover cosmic strings [9], boson stars [10] and neutralino stars [11],[12] through their gravitational lensing effects. There is no compelling evidence that any of the observed GL systems are due to these objects, however, it is essential to develop new lens models with objects which are though not yet observed, but not forbidden on the theoretical grounds. In the present paper we investigate gravitational lensing of an empty gravity ball situated at a cosmological distance. The lens—gravity ball—has interesting features which are not shared by other known lenses. The lensing effect is radically different—rays with impact parameter greater than the radius of the ball are not deflected.

The paper is organised as follows. In the Section 2 we give the general formalism of the problem for a gravity ball, in the Section 3 we discuss the effect of GL by gravity ball, namely, the number of images, magnification, etc. Finally in the last section we give the conclusions.

2. General formulations

Gravity ball as a NTS solution

Here we will discuss the general formalism of the problem for a spherically symmetric system consisting of fermion field ψ , scalar field σ and gravitational field $g_{\mu\nu}$. We follow the theory presented by Sethi and Lohiya [8]. Gravity balls are the NTS solutions of the field equations arising from (1)

$$U(\sigma)[R^{\mu\nu} - \frac{1}{2}g^{\mu\nu}R] = -\frac{1}{2}[T_{\omega}^{\mu\nu} + T_{\sigma}^{\mu\nu} + T_{\sigma,\psi}^{\mu\nu} + T_{\psi}^{\mu\nu} + 2U(\sigma)^{;\mu;\nu} - 2g^{\mu\nu}U(\sigma)_{;\lambda}^{\lambda}]$$

$$g^{\mu\nu}\sigma_{;\mu;\nu} + \frac{\partial V}{\partial\sigma} - R\frac{\partial U}{\partial\sigma} = 0 \quad (2)$$

Here $T_{\sigma}^{\mu\nu}$, $T_{\psi}^{\mu\nu}$, $T_{\sigma,\psi}^{\mu\nu}$ and $T_{\omega}^{\mu\nu}$ are energy momentum tensors constructed from action for the scalar field, the

fermion field, together with its Higgs coupling to σ , and the rest of the matter fields, respectively. We consider an NTS with the scalar field held to a value σ_0 in the interior and making a fast transition to $\sigma = 0$ outside a thin shell. Thus, we have essentially three regions, interior of a soliton ($r < R_0$), a shell of thickness $\sim \mu^{-1}$ and surface energy density $s \approx \mu\sigma_0^2/6$, and exterior ($r > R_0$). The total energy of a NTS has contributions from: (1) the surface tension energy $E_s \approx sR_0^2$; (2) the energy of the fermions $E_f \approx N^{4/3}/R_0$ and; (3) the volume energy $E_V \approx V(\sigma_{in})R_0^3$. For the degenerate case $V(\sigma_{in}) = 0$, a NTS has total mass constrained by the stability against gravitational collapse to a value determined by the surface tension s . The soliton mass, obtained by minimizing the total energy, is $M = 12\pi sR_0^2$. For $s \sim (MeV)^3$ and $N \approx 10^{75}$, the size of the NTS is of the order of tens of kiloparces, while it is still away from the Schwarzschild bound. For configurations with R much greater than the Schwarzschild radius, the effects of gravity can be treated as a small perturbation. Thus, the form of the metric for the NTS satisfies a “weak field approximation”.

A. Interior: $r < R_0 + \mathcal{O}(\mu^{-1})$. The metric inside is described as

$$ds^2 = e^{2u(r)} dt^2 - e^{2v(r)} dr^2 - r^2[d\theta^2 + \sin^2\theta d\varphi^2] \quad (3)$$

The interior metric has one specific solution:

$$v = -\frac{\hat{C}r^2}{6}$$

and

$$u = u_0 + \frac{r^2}{2} \left[\frac{\tilde{C}}{2} + \frac{\hat{C}}{3} \right] \quad (4)$$

with \tilde{C} and \hat{C} —constants depending on the fermionic energy inside the soliton. In the weak field approximation used here we consider the interior with

$$ds^2 \approx e^{2u_0} dt^2 - dr^2 - r^2[d\theta^2 + \sin^2\theta d\varphi^2] \quad (5)$$

B. Exterior: $r > R_0 + \mathcal{O}(\mu^{-1})$. In the exterior region we have essentially Minkowskian metric

$$ds^2 = dt^2 - dr^2 - r^2[d\theta^2 + \sin^2\theta d\varphi^2] \quad (6)$$

To be consistent with the observations we will see that the u_0 has to be small negative constant. The propagation of light inside the G-ball is equivalently described by using the Fermat principle with the effective refraction index n_{eff} inside the ball given by

$$n_{eff} = 1 - u_0 \quad (7)$$

This gives straight trajectories of light rays inside the ball. But since outside the ball $n_{eff} = 1$, we see that G-ball behaves as a spherical lens (deflection of light occurs only at the boundaries).

3. Lens Model for a G-ball and Lensing Properties

Throughout the paper, we employ the conventions of many articles, reviews and books on gravitational lensing (see, for example, [13], [14]) and which are essentially illustrated in the Fig.1.

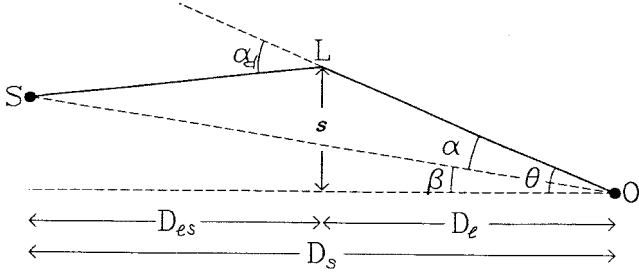


Figure 1: Basic geometry of gravitational lensing. The light ray propagates from the source S to the observer O , passing the lens L at transverse distance s . Angle α_d is the angle of deflection. The angular separations of the source and the image from the optic axis as seen by the observer are β and θ , respectively. The distances between the observer and the source, the observer and the lens, the lens and the source are D_s , D_l and D_{ls} , respectively.

The positions of the source and the image are related through the *lens equation*

$$\vec{\beta} = \vec{\theta} - \frac{D_{ls}}{D_s} \vec{\alpha}_d \quad (8)$$

where we employ angular diameter distances. We restrict our discussion to a cosmological model which is a variant of a Milne universe [8] with a scale factor $R(t) = t$ and cosmological parameters $\Omega_0 = 0$, $\Omega_\Lambda = 0$. In this cosmology angular diameter distances are given by

$$D_l = \frac{cz_l (2 + z_l)}{2H_0 (1 + z_l)^2} \quad (9)$$

$$D_s = \frac{cz_s (2 + z_s)}{2H_0 (1 + z_s)^2} \quad (10)$$

$$D_{ls} = \frac{cz_{ls}}{2H_0 (1 + z_l) (1 + z_{ls})^2} \quad (11)$$

with

$$z_{ls} = \frac{z_s - z_l}{1 + z_l} \quad (12)$$

and $H_0 = 100 h \text{ km s}^{-1} \text{ Mpc}^{-1}$ is the Hubble constant. Subscripts l , s and ls stand for lens, source and lens-source, correspondingly.

In our subsequent development we also utilize the following assumptions, mostly related to the modelling

of the deflector. We consider the gravity ball to be of the size of a typical cluster of galaxies at the cosmological distance and embedded in the empty space—region with no matter concentrations close to it. The deflector is transparent. We also assume a thin lens approximation since all deflection occurs within $\Delta z \leq \pm R_0$; the extent of the deflector is thus taken to be small compared with its distance from both the observer and the source (say, distances from us to the cluster at $z = 0.3$ and to the source at $z = 1$ are $\sim 1 \text{ Gpc}$ and $\sim 2 \text{ Gpc}$, respectively, while $R_0 \approx 0.5$ to 1 Mpc). We regard deflection angles to be small. We also assume that the positions of the source, lens, and observer are stationary with respect to comoving coordinates.

The magnification of images is given by

$$\mu = \left| \det \frac{\partial \vec{\beta}}{\partial \vec{\theta}} \right|^{-1}$$

which in axisymmetric case goes to

$$\mu = \left(\frac{\beta d\beta}{\theta d\theta} \right)^{-1} \quad (13)$$

The tangential and radial critical curves follow from the singularities of the tangential and radial magnification

$$\mu_t \equiv \left(\frac{\beta}{\theta} \right)^{-1} \quad (14)$$

$$\mu_r \equiv \left(\frac{d\beta}{d\theta} \right)^{-1} \quad (15)$$

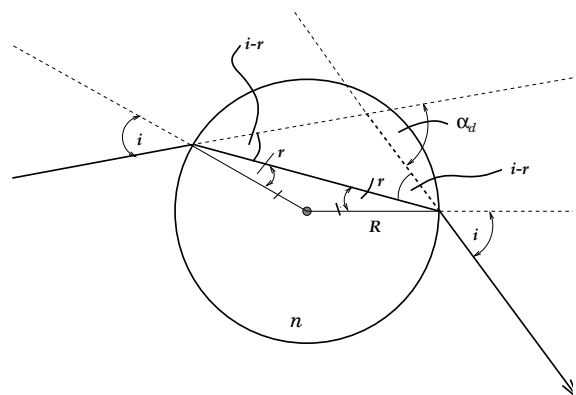


Figure 2: R_{ball} —radius of the ball, i —angle of incidence, r —angle of refraction, α_d — deflection angle, n —ratio of the refractive index inside the ball to the refractive index outside; $n > 1$.

Lens equation. In the Fig. 2 we present the geometry of G-ball as a lens. From the Fig.2 and Snell's law the deflection angle α_d is

$$\alpha_d = 2 \left[i - \sin^{-1} \left(\frac{1}{n} \sin i \right) \right] \quad (16)$$

Since we consider all angles to be small, the following approximations are valid. Defining the quantity

$$\theta_C = \frac{R_{ball}}{D_l} \quad (17)$$

which is the radius of the region inside which the refraction occurs, we obtain the expression for the deflection angle α_d

$$\alpha_d = 2 \left[\sin^{-1} \left(\frac{\theta}{\theta_C} \right) - \sin^{-1} \left(\frac{\theta}{n\theta_C} \right) \right] \quad (18)$$

Plugging (18) into the general lens equation (8) we obtain lens equation for the gravity ball

$$\vec{\beta} = \vec{\theta} - \frac{2D_{ls}}{D_s} \frac{\vec{\theta}}{\theta} \left[\sin^{-1} \left(\frac{\theta}{\theta_C} \right) - \sin^{-1} \left(\frac{\theta}{n\theta_C} \right) \right]$$

$$\text{for } 0 \leq \theta \leq \theta_C \quad (19)$$

and

$$\vec{\beta} = \vec{\theta}$$

$$\text{for } \theta > \theta_C, \quad (20)$$

where $\theta \equiv |\vec{\theta}| = \sqrt{\theta_1^2 + \theta_2^2}$ is the radial position of the image in the lens plane.

Multiple image diagram and conditions for multiple imaging. To illustrate the lensing properties described by equations (19,20) we show in Figure 3 the lensing curve for the gravity ball with parameters $n = 1.0005$, $\theta_C = 5'$ and for $z_{source} = 1$, $z_{lens} = 0.3$. The intersections of the lines $\beta = const$ with the curve given by equation (19) give the solutions to the lensing equation. The source at β_2 lies on a caustic point and θ_r is the radius of the radial critical curve; the source at β_1 has three images; and point $\beta = 0$ produces a ring—‘Einstein ring’—with the critical radius $\theta = \theta_t$ and an image at $\theta = 0$. The function $\beta(\theta)$ is continuous except at θ_C due to the edge of the ball.

Putting $\beta = 0$ in (19) gives

$$\theta - \frac{2D_{ls}}{D_s} \left(\sin^{-1} \frac{\theta}{\theta_C} - \sin^{-1} \frac{\theta}{n\theta_C} \right) = 0 \quad (21)$$

Denoting $a = 2D_{ls}/D_s$

$$\theta = a \left(\sin^{-1} \frac{\theta}{\theta_C} - \sin^{-1} \frac{\theta}{n\theta_C} \right) \quad (22)$$

When the alignment of the source, lens and the observer is not perfect, we see the features called arcs, which are the result of very strong distortion of a background sources. Arcs roughly trace the Einstein ring, so $\theta_{arc} \approx \theta_E$. Since radii of most known arcs do not exceed $30''$ small angle approximation is valid and we obtain

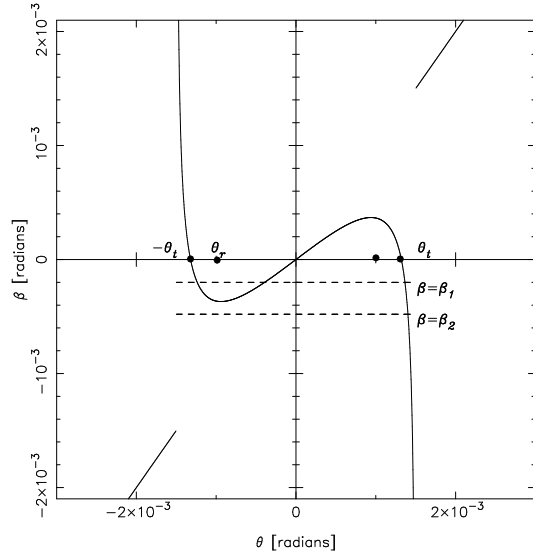


Figure 3: Solution to the lensing equation by a gravity ball. The solid curve represents the lensing equation curve with $n = 1.0006$, $\theta_C = 5'$, $z_{source} = 1$, $z_{lens} = 0.3$, together with lines $\beta = \beta_i$ (dashed lines) for various source positions β_i . The intersections of the lines $\beta = const$ with the lensing equation curve give the number and positions of the lensed images. The source at β_2 lies on a caustic point and θ_r is the radius of the radial critical curve; source at β_1 has three images and point $\beta = 0$ produces a ring $\theta_C = \theta_t$; in addition, it has an image at $\theta = 0$. The function $\beta(\theta)$ is continuous except at θ_C due to the edge of the ball.

$$\theta \left\{ 1 - \frac{a}{\theta_C} \sqrt{1 - \left(\frac{\theta}{n\theta_C} \right)^2} + \frac{a}{n\theta_C} \sqrt{1 - \left(\frac{\theta}{\theta_C} \right)^2} \right\} = 0 \quad (23)$$

One solution to this equation is trivial:

$$\theta = 0 \quad (24)$$

which corresponds to the image located at the centre of the lens. To find other solutions we write the expression in the curly brackets in (23) as

$$\theta = \theta_C \sqrt{1 - \frac{a^2 n^2}{4\theta_C^2} \left(1 - \frac{\theta_C^2}{a^2} - \frac{1}{n^2} \right)^2} \quad (25)$$

and in order to find the conditions for the Einstein ring we rewrite it in the form

$$\theta_E = \theta_C \sqrt{1 - \frac{a^2 n^2}{4\theta_C^2} \left(1 - \frac{\theta_C^2}{a^2} - \frac{1}{n^2} \right)^2} \quad (26)$$

Assuming for simplicity $a = 1$ (the ball (lens) is half-way between the observer and the source) and using

n from other estimates [8] to be from 1.001 to 1.0001 we obtain

for $n = 1.0001$

$$\theta_E \cong 0.98 \theta_C \quad (27)$$

for $n = 1.001$

$$\theta_E \cong 0.73 \theta_C \quad (28)$$

Here θ_E is non-trivial solution of the equation (23). This leads to the appearance of the image in the form of a ring with the radial size of ~ 0.9 to 0.7 of the total size of the ball, depending on n . To find the condition for the appearance of multiple images we analyze (25). To obtain a physical solution we take

$$1 - \frac{a^2 n^2}{4\theta_C^2} \left(1 - \frac{\theta_C^2}{a} - \frac{1}{n^2} \right)^2 > 0 \quad (29)$$

The conditions for multiple imaging are

$$R_{ball} > 2D_{eff} \left(1 - \frac{1}{n} \right) \quad (30)$$

or expressed through n

$$1 < n < \frac{2D_{eff}}{2D_{eff} - R_{ball}} \quad (31)$$

where $D_{eff} = \frac{D_s D_l}{D_s}$ is effective distance.

Magnification and critical curves. From lens equation for a G-ball (19) and equation (13) we obtain expression for the total magnification of the images

$$\mu^{-1} = \left\{ 1 - \frac{a}{\theta} \left[\sin^{-1} \left(\frac{\theta}{\theta_C} \right) - \sin^{-1} \left(\frac{\theta}{n\theta_C} \right) \right] \right\} \times \left\{ 1 - a \left(\frac{1}{\sqrt{\theta_C^2 - \theta^2}} - \frac{1}{\sqrt{n^2 \theta_C^2 - \theta^2}} \right) \right\} \quad (32)$$

where first term represents μ_t and second term— μ_r . In Figure 4 we have plotted tangential magnification μ_t and radial magnification μ_r against θ for a G-ball with refraction index $n = 1.001$. Singularities in these give the angular positions of tangential critical curves and radial critical curves, respectively. In the same Figure we also plotted total magnification μ vs. θ .

Limits on n from observations. We can rewrite equation (26) in terms of variables R_{ball} and R_E to get an expression for R_{ball} in terms of n and a given R_E .

$$R_{ball}^2 = 4D_{eff} \left[1 + \frac{1}{n^2} - \frac{\sqrt{4D_{eff}^2 - R_E^2}}{nD_{eff}} \right] \quad (33)$$

Since $R_{ball} \geq R_E$, we get a lower bound on the value of R_{ball} if we know the radius of the Einstein's ring. It is clear from the above equation that if the size of

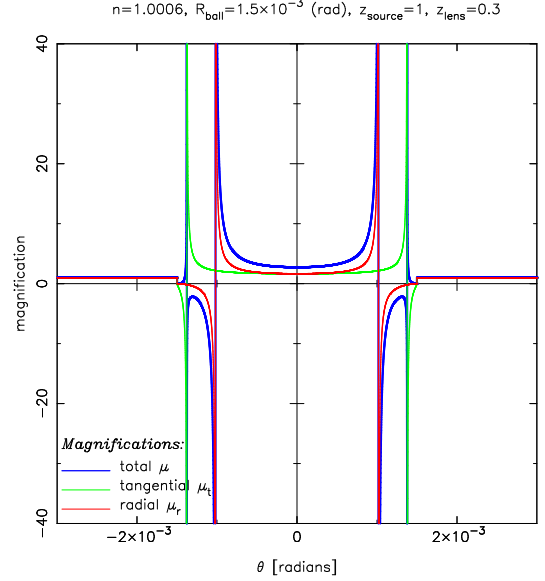


Figure 4: The magnifications: tangential μ_t denoted by green, radial μ_r denoted by red, and total μ is shown by blue line. Curves are plotted as a function of the image positions θ for the parameters of the lens: $n = 1.0006$, $\theta_C = 5'$, $z_l = 0.3$, $z_s = 1$. The singularities of μ_r and μ_t give positions of the tangential and radial critical curves, respectively.

the G-ball is big enough then a large enough n can give us any desired radius for the Einstein's ring. If we assume that all G-balls are of the same size then from observations we can infer a lower bound on the radius and the refractive index inside a ball by the following argument. The radius of any gravity ball has to be larger than the radius of the largest observable Einstein's ring. Given this size of the ball the refractive index should be large enough to give a real Einstein's ring for every other case. This situation is illustrated in the Figure 5, where observational data for few clusters with giant arcs (details are presented in the Table 1) are used with the assumption that the radius of the arc $\theta_{arc} \approx \theta_E$. Together with the curve (33) for the cluster A370 we plotted the value of the radius R_{arc} of the A5 arc in that cluster (horizontal line), which is the largest amongst presented clusters. It is clear that the refractive index should be greater than the value where this line intersects the $R_{ball}-n$ curve for this cluster. Assuming R_{ball} to be the same, we can see that in order to have an arc, a gravity ball must have n more than $n \approx 0.00056$. Thus, we obtained a lower limit on n . Of course, our present calculations are for the case of empty gravity ball. Matter concentrations in the centre of the ball increase the deflection angle. We intend to explore in details this analysis in our next paper.

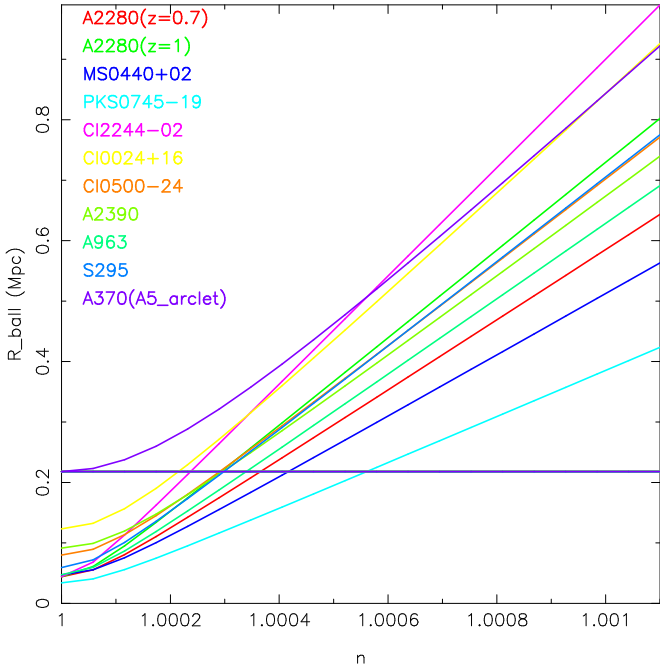


Figure 5: R_{ball} vs. n for different clusters. Clusters are marked by different colours. Corresponding curves have the same colour as the name of the cluster. Details are presented in Table 1. Horizontal line is the value of radius of the arc A5 in the cluster A370.

Simulations. To demonstrate how a G-ball at intermediate redshift gravitationally distorts background sources we performed computer simulations and presented the results in Figures 6 and 7. We simulated empty gravity ball of a size of a typical galaxy cluster at the redshift of $z_l = 0.3$. We assumed for simplicity that all source galaxies are at the same redshift $z_s = 1$. The luminous area of each background galaxy is taken to be a circular disk of radius R with constant brightness. In all our numerical computations we used Hubble parameter $h = 1$. For the simulations of G-ball lensing we use the algorithm described in [13]. The image configurations by a simulated gravity ball are illustrated in Figure 6 by changing the relative positions between the extended circular source and the lens. When the alignment of the source on the optical axis is perfect, the ring image—Einstein ring—appears (Fig.6a); with a small displacement we see two opposite arcs approximately located at the Einstein radius (Fig.6e). When the displacement becomes larger different features may appear: single tangential arc Fig.6(b), radial arc (Fig. 6(d), two opposite images (Fig. 6(c) and straight arc (Fig.6(f)). Figure 7 displays the distortion the gravity ball produces on the field of randomly distributed background sources. Figure 7(a) shows an unperturbed galaxy background projected randomly in a field of $\sim 10' \times 10'$ at a redshift of $z = 1$. Fig. 7(b) illustrates the same field with an empty G-ball at the

centre. To compare with the lensing effect a cluster modelled as a singular isothermal sphere produces on the background galaxies, we presented in the Fig.7(c) the simulation taken from the [15]. We can see from the figures that an empty gravity ball can indeed act as a strong lens and produce the images of arcs and arclets.

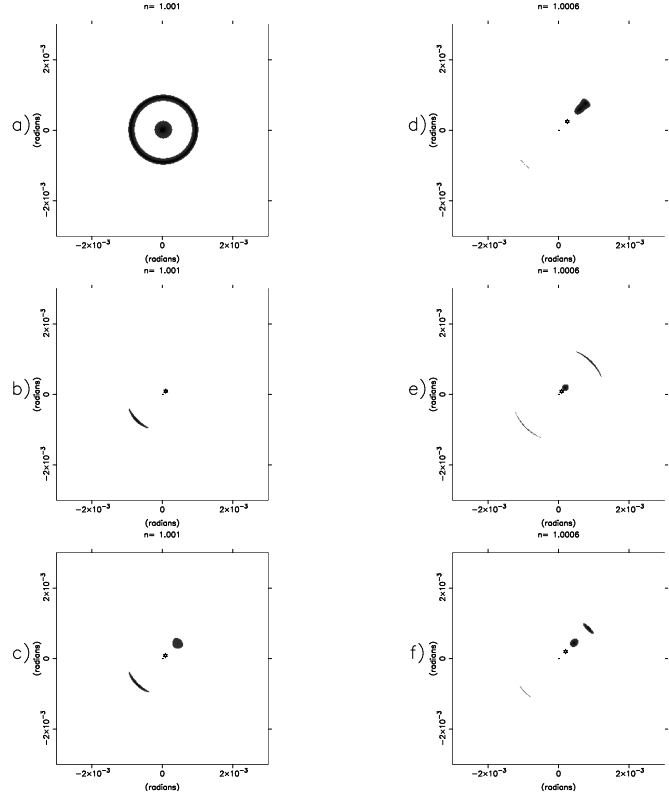


Figure 6: Illustration of six different imaging situations for an empty gravity ball. $z_l = 0.3$, $z_s = 1$, $\theta_C = 5'$. Depending on the source position and n the lens produces images of (a) ring, (b) single arc, (c) arc and opposite image, (d) radial arc, (e) three images (with two opposite arcs), (f) two images on one side (with a straight arc). Small dot in the centers of the panels marks the center of the G-ball. Small star marks the position of the source.

4. Conclusions.

In the present paper we have discussed a special kind of nontopological soliton, known as gravity ball, and examined the possibility for it to be a gravitational lens. We investigated its lensing properties, calculated the deflection angle of a point source, derived the lens equation and plotted the lens curve for the gravity ball with specific parameters. We have shown that depending on the parameters of the model there can be one, two or three images (two inside the Einstein radius and one outside). However, the G-ball gravita-

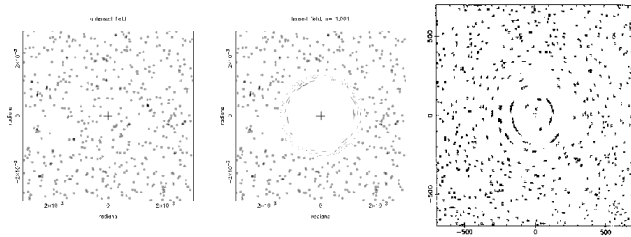


Figure 7: Distortion field generated by the simulated gravity ball. The left panel shows the grid of randomly distributed background sources as it would be seen in the absence of the lens. The middle panel shows the same population once they are distorted by a foreground gravity ball with the parameters: $z_s = 1$, $z_l = 0.3$, $\theta_C = 5'$ rad, $n = 1.001$. The right panel shows the same population distorted by a foreground (invisible) circular cluster ($z_s = 1.3$, $z_l = 0.4$, $\sigma = 1000 \text{ km s}^{-1}$). The simulation in the right panel is taken from [15] and the units for both axis are in arcsecs.

tional lens has interesting features which are not shared by other known gravitational lenses. In the case of a source, lens and observer located on the optical axis together with the Einstein ring there is always an image in the centre. Besides, the lensing geometry is radically different—there is no effect outside the lens and thus, Einstein radius is always less than radius of the ball. The refractive index of the gravity ball contributes to the decrease in the radius of the Einstein ring and increase of its thickness. For the extended sources we showed how a large gravity ball can induce surprisingly large distortions of images of distant galaxies. It is assumed that in order to produce large arcs the cluster must have its surface-mass density approximately supercritical, $\Sigma \geq \Sigma_{crit}$. We found that the empty balls alone are able to produce arc-like features, including straight arcs, arclets and radial arcs. We have modelled the gravitational lensing effect of our gravity ball on a background source field and found that the ball produces distortion (‘shear’) of that field, consistent to some extent with the observations. We also obtained constraints on the size of the large gravity ball, which can be inferred from the existing observations of clusters with arcs. Empty G-balls can show in observations as arcs without evident mass distribution—a lens and/or through the distortion of the background random galaxy field. Clearly, there are factors that this analysis has not taken into account, for example, the gravity ball with the complex mass distribution inside. These issues will be addressed in future papers.

Observationally empty G-balls have not yet been found, but we conclude from our preliminary analysis that the existence of large G-balls cannot be ruled out by gravitational lensing effects.

Acknowledgements

MS is supported by a ICCR scholarship (Indo-Russian Exchange programme) and acknowledges the hospitality of IUCAA, Pune. We would like to deeply thank Tarun Deep Saini for his expert assistance with the software.

References

- [1] G. B. Gelmini, M. Gleiser and E. W. Kolb, *Phys. Rev. D.*, **39** (6), 1558 (1989).
- [2] B. Holdom, *Phys. Rev. D*, **36**, 1000 (1986).
- [3] A. D. Dolgov and O. Yu. Markin, *Sov. Phys. JETP*, **71**, 207 (1990).
- [4] S. Coleman, *Nucl. Phys.*, **B262**, 263 (1985).
- [5] T. D. Lee and Y. Pang, *Phys. Rev. D.*, **35**, 3678 (1987), and references therein.
- [6] T. D. Lee and G. C. Wick, *Phys. Rev. D*, **9**, 229 (1974).
- [7] R. Friedberg, T. D. Lee and A. Sirlin, *Phys. Rev. D.*, **13**, 2739 (1976); *Nucl. Phys.* **B115**, 1 (1976); **B115**, 32 (1976).
- [8] M. Sethi and D. Lohiya, *Class. Quan. Grav.*, 1545, (1999).
- [9] A. Vilenkin, *Ap. J.*, **L51**, 282 (1984).
- [10] M. P. Dabrowski and F. E. Schunck, *astro-ph/9807039*.
- [11] M. V. Sazhin et al, *Phys. Let. A.*, **215**, 199 (1996).
- [12] M. V. Sazhin, A. G. Yagola, A. V. Yakubov and A. F. Zakharov, *Astroph. Space Sci.*, **252**, 365 (1997).
- [13] P. Schneider, J. Ehlers and E. E. Falco, *in*: “Gravitational lenses”, Heidelberg: Springer 1992.
- [14] A. F. Zakharov and M. V. Sazhin, *Physics–Uspekhi*, **41**, 945 (1998).
- [15] B. Fort and Y. Mellier, *Astron. Astroph. Rev.*, **5**, 239 (1994).

Table 1: Lensing cluster sample

Table 1. Lensing cluster sample

<i>cluster</i>	z_{cl}	<i>arc</i> ^a	z_{arc}	r (arcsecs) ^b	<i>ref.</i> ^c
A2280	0.326	large arc	≈ 0.7 or 1.0?	14''	1
MS 0440+0204	0.190	1 GLA + 3 bright arcs	0.53?	22''	2
A370	0.374	arclet A5	1.306?	63.7''	3
PKS 0745-191	0.1028	bright arc	0.433	18.2''	4
A2390	0.231	GLA; straight image	0.913	37''	5
A963	0.206	GLA+counter arc	0.77	image separation= 30''; $R_E = 15''$	6
Cl 2244-02	0.329	GLA	2.237	14''	7
Cl 0024+1654	0.391	five arcs	1.39?	35''	8
Cl 0500-24	0.316	GLA	0.913	$\sim 26''$	9
S295	0.299	GLA	0.93	$\sim 20''$	10

^a Lensing phenomenon. GLA–giant luminous arc.

^b Distance from the centre of cluster where arc(s) are detected.

^c Only one reference is provided for lensing feature.

References

1. I. M. Gloia et al, *Astron. Astrophys.*, **297**, L75 (1995).
2. G. A. Luppino et al, *Ap.J.*, **416**, 444 (1993).
3. I. Smail et al, *Mon. Not. R. Astron. Soc.*, **252**, 19 (1991).
4. S. W. Allen, A. C. Fabian and J. P. Kneib, *Mon. Not. R. Astron. Soc.*, **279**, 615 (1996).
5. R. Pello et al, *Ap.J.*, **366**, 405 (1991)
6. R. J. Lavery and J. P. Henry, *Ap.J.*, **329**, L21 (1988)
7. S. A. Grossman and P. Saha, *Ap.J.*, **431**, 74 (1994)
8. W. N. Colley, J. A. Tyson and E.L. Turner, *Ap.J.*, **461**, L83 (1996)
9. E. Giraud, *Ap.J.*, **334**, L69 (1988)
10. A. C. Edge et al, *Astron. Astrophys.*, **289**, 1 (1994).